UK/95-01
Jan. 1995
hep-ph/9502334

Flavor-Singlet g_A from Lattice QCD

S.J. Dong, J.-F. Lagaë, and K.F. Liu

Dept. of Physics and Astronomy
Univ. of Kentucky, Lexington, KY 40506

Abstract

We report on a lattice QCD calculation of the flavor-singlet axial coupling constant g_A of the proton from the axial-vector current. The simulation is carried out at $\beta = 6$ on a quenched $16^3 \times 24$ lattice. An extrapolation to the chiral limit shows that the connected insertion (valence and cloud parts) is 0.62 ± 0.09, which is close to g_A^8. The disconnected insertion (vacuum polarization from the sea quark) for the u or d quark is -0.12 ± 0.01 and the s quark also contributes -0.12 ± 0.01. The total g_A^1 is thus 0.25 ± 0.12 which is in agreement with experiments. In addition, we find $g_A^3 = 1.20 \pm 0.11$, $g_A^8 = 0.61 \pm 0.13$ and $F_A/D_A = 0.60 \pm 0.02$, also in agreement with experiments.

PACS numbers: 12.38.Gc, 14.20.Dh, 13.60.Hb, 12.38.-t

Recent experiments on polarized deep inelastic lepton-nucleon scattering from SMC [1] and E143 [2] have confirmed the finding of the earlier EMC [3] results that the flavor-singlet g_A^1 is small [4]. In the deep inelastic limit, the integral of the polarized structure function is related to the forward matrix elements of axial currents from the operator product expansion [5]. Combined with the neutron and hyperon decays, the flavor-singlet axial coupling g_A^1 is extracted. Since the axial current is the canonical spin operator, g_A^1 is thus the quark spin content of the nucleon; i.e. $g_A^1 = \Delta u + \Delta d + \Delta s$, where the spin content $\Delta q (q = u, d, s)$ is defined in the forward matrix element of the axial current, $\langle ps|\bar{q} i \gamma_\mu \gamma_5 q|ps\rangle = 2 M_N s_\mu \Delta q$.

The fact that g_A^1, which represents the quark spin contribution to the proton spin, is found to be much smaller than the expected value of unity from the non-relativistic quark model or 0.75 from the SU(6) relation (3/5 of the isovector coupling $g_A^3 = 1.2574$) has attracted a lot of attention. Despite numerous attempts [6] to explain the smallness of g_A^1 by means of various hadronic models, effective theories, and anomalous Ward identity [7], this problem has persistently defied satisfactory answer and has been dubbed the "proton spin crisis".

Attempts have also been made to calculate g_A^1 via the anomalous Ward identity using lattice QCD, which is well poised for such a challenge [8, 9]. However, it has been pointed out [8, 7] that in the quenched approximation, the induced pseudoscalar coupling can not be ignored due to the would-be Goldstone boson dominance in the forward matrix element. As a result, the topological coupling to the nucleon $\langle N|G\tilde{G}|N\rangle$ is not directly related to g_A^1 in the quenched approximation. Lattice calculations with dynamical fermions are free of this problem. Modulo uncertainties from the chiral and zero momentum extrapolation, a recent calculation of the topological coupling of the nucleon using dynamical staggered fermions [9] shows that the quark spin content is indeed small, comparable to the experimental findings. However, a calculation of g_A^1 via the Ward identity does not address the issue why it is much smaller than that of the quark model, a question which is at the heart of the spin crisis. In an attempt to answer this question, we carry out a lattice calculation of the axial current directly. It turns out that the polarization due to the degrees of freedom outside of the naive quark model, i.e. cloud and sea quarks, are responsible for the smallness of g_A^1.

Lattice calculations of three-point functions have been used to study the EM [10], axial (isovector) [11], and pseudoscalar(πNN) [12] form factors of the nucleon. For the flavor-singlet g_A^1, we calculate the following two- and three-point functions,

$$G_{PP}^{\alpha\alpha}(t) = \sum_{\vec{x}} \langle 0|\chi^\alpha(x)\bar{\chi}^\alpha(0)|0\rangle \tag{1}$$

$$\Gamma_3^{\beta\alpha} G_{PA_3P}^{\alpha\beta}(t_f, t) = \sum_{\vec{x}_f, \vec{x}} \Gamma_3^{\beta\alpha} \langle 0|\chi^\alpha(x_f) A_3(x) \bar{\chi}^\beta(0)|0\rangle, \tag{2}$$

where χ^α is the proton interpolating field, $\Gamma_3 = -i\gamma_3\gamma_5(1+\gamma_4)/2$, and A_3 is the

point-split axial current from the Wilson action

$$A_\mu = 2\kappa f(ma)[\bar{\psi}(x)\frac{1}{2}i\gamma_\mu\gamma_5 U_\mu(x)\psi(x+\hat{\mu}) + \bar{\psi}(x+\hat{\mu})\frac{1}{2}i\gamma_\mu\gamma_5 U_\mu^\dagger(x)\psi(x)]. \qquad (3)$$

In contrast to the isovector case, the evaluation of the three-point function for the flavor-singlet current involves a *disconnected insertion*(DI) in addition to the *connected insertion*(CI) [7]. The quark line skeleton diagrams for the CI and DI are shown in Fig. 1(a) and 1(b) respectively. The DI refers only to the quark lines. They are nonetheless correlated via the background gauge fields. We shall calculate the CI and DI separately. The factor $f(ma)$ in eq. (3) is the finite ma correction for the Wilson action. We take $f(ma) = e^{ma} = (4\kappa_c/\kappa - 3)$ for the connected insertion. For the disconnected insertion, the factor $f(ma)$ is different from e^{ma} and depends on the Lorentz structure of the current. We shall use the value of $f(ma)$ computed by comparing the triangle diagram in the lattice Wilson action and the continuum [14].

The connected insertion is calculated in the same way as the isovector axial coupling g_A^3 [11] where eqs. (1) and (2) are fitted to two exponentials in the form $fe^{-mt'_f}$ and $g_{A,con}^{1L} fe^{-mt_f}$ simultaneously, using the data-covariance matrix to account for correlations. In evaluating the three-point function, the factor $8\kappa_c\langle\frac{1}{3}TrU_{plaq}\rangle^{1/4}$ ($\kappa_c = 0.1568$) is divided from the axial current in eq. (3) to account for the mean-field improvement of the lattice operator [13, 11, 12]. Numerical details are given in Ref. [11]. The unrenormalized lattice $g_{A,con}^{1L}$ has been calculated for $\kappa = 0.154, 0.152$, and 0.148, corresponding to quark masses of about 120, 200, and 370 MeV respectively (the scale $a^{-1} = 1.74(10)$GeV is set by the nucleon mass), and is plotted in Fig. 2. The calculations were done on a quenched $16^3 \times 24$ lattice at $\beta = 6.0$ with 24 gauge configurations as in the isovector case [11]. Extrapolation to the chiral limit ($\kappa_c = 0.1568$) yields $g_{A,con}^{1L} = 0.65 \pm 0.09$ as shown in Fig. 2. The g_A^1 in the continuum is related to its lattice counterpart by the relation $g_A^1 = Z_A g_A^{1L}$, where Z_A is the finite lattice renormalization constant. The one-loop calculation gives $Z_A = 0.952$ for $\beta = 6.0$ [13], from which we find $g_{A,con}^1 = 0.62 \pm 0.09$.

First we note that $g_{A,con}^1 = \Delta u_{con} + \Delta d_{con}$ is the OZI preserving part of g_A^1. If the DI part (sea-quark contribution) is roughly flavor-independent, i.e. $\Delta u_{dis} = \Delta d_{dis} \simeq \Delta s$ (strange quarks appear only in DI), as will be shown below, then $g_{A,con}^1$ should be close to g_A^8, the octet axial coupling, i.e.

$$g_A^8 = \Delta u_{con} + \Delta d_{con} + (\Delta u_{dis} + \Delta d_{dis} - 2\Delta s) \simeq g_{A,con}^1 \qquad (4)$$

From the recent fit of the nucleon and hyperon β decays, $g_A^8 = 0.579 \pm 0.021$ [15]. We see that our calculated $g_{A,con}^1$ is quite in agreement with this. Second, we notice that the calculated ratio $R_A = g_{A,con}^1/g_A^3$ is smaller than the expected value of 3/5 from the SU(6) relation of the relativistic quark model. The behavior of this ratio R_A is plotted in Fig. 3 as a function of the quark mass. For heavy quarks (at ma = 1, m = 1.74 GeV), R_A is 3/5. This is to be expected of the non-relativistic quarks where $g_A^3 = 5/3$ and $g_A^1 = 1$. For light quarks, R_A becomes progressively less than 3/5. It has been shown [16] that this deviation from the SU(6) relation is due to

the presence of cloud quarks and antiquarks (those in the higher Fock space than the valence in the CI). When this degree of freedom is eliminated by disallowing quarks from propagating backward in time, it is found that R_A becomes 3/5 (shown as dots in Fig. 3 where the errors are smaller than the dot size). The SU(6) relation is therefore recovered in the *valence approximation*, in which the Fock space is limited to the valence quarks. We should mention that under this valence approximation, the quark spin content is still not equal to the non-relativistic value of unity. This has been explained [17] as a relativistic effect. Owing to the presence of the lower component in the Dirac spinor, a confined quark with s-wave upper component still has a non-vanishing orbital angular momentum. Thus we conclude that the reason $g^1_{A,con}$ is only about 60% of the non-relativistic value of 1 is because of relativistic effects and polarization due to cloud quarks and antiquarks.

To calculate the DI in Fig. 1(b), we sum the ratio between eq. (2) and eq. (1) over t. It has been shown [18] that as $t_f >> a$, this sum becomes

$$\frac{1}{3}\sum_{i=1}^{3}\sum_{t}\frac{\Gamma_i^{\beta\alpha}G^{\alpha\beta}_{PA_iP}(t_f,t)}{G^{\alpha\alpha}_{PP}(t_f)} \underset{t_f>>a}{\longrightarrow} \text{const} + t_f g^{1L}_{A,dis} \tag{5}$$

Thus, we calculate the sum as a function of t_f and take the slope to obtain the DI part of g^1_A. Since the DI involves quark loops, and thus entails the calculation of off-diagonal traces of the inverse quark matrix, it poses a challenging numerical problem, for the size of the quark matrix is as large as $10^6 \times 10^6$ in the present case. In [19], we developed an efficient algorithm to estimate these traces stochastically with Z_4 noise, which gives the estimate with the minimum variance. This algorithm has been tested by computing quantities for which the exact answers are known. We have checked the cases of DI with vector and pseudoscalar currents. In both of these cases, the matrix elements are proportional to the 3-momentum transfer q. Hence, the forward matrix elements should vanish. Presented in Fig. 4 are results of the ratios in eq. (5) for the corresponding currents. These are obtained with 300 Z_4 noise vectors in each of the 50 gauge configurations for $\kappa = 0.148$. To avoid contaminations by the boundary effects introduced by the fixed boundary condition we imposed in the time direction, we summed t from the nucleon source, which is 4 time slices away from the boundary, to 4 time slices from the other boundary. The slopes of the ratios (indicated as ME in Fig. 4) are fitted from the point where the nucleon emerges as a single exponential in the two-point function which is at $t = 8$ and onward. We see that for both the vector and pseudoscalar cases, the calculated forward m.e. are indeed consistent with zero. We also calculated the scalar m.e. $\langle N|\bar{q}q|N\rangle_{dis}$. We see that the slope is large and positive, and thus has the right magnitude and sign to remove the discrepancy between the $\pi N\sigma$ term calculated from πN scattering and those lattice calculations with only the CI. Similarly, the corresponding results for $\kappa = 0.154$ are shown in Fig. 4. This is the lightest quark we considered and it yields the largest errors. However, the forward m.e. for the vector and pseudoscalar currents are still consistent with zero and the scalar m.e. is larger than that of $\kappa = 0.148$. We conclude from this study that stochastic estimation with Z_4 noise produces the correct results within errors.

Having tested our algorithm against known quantities, we proceed to calculate the axial-vector current. The results for $\kappa = 0.148, 0.152$ and 0.154 are presented in Fig. 5. They are obtained in the following way. First, the slopes are fitted in the region $t_f \geq 8$ where the nucleon is isolated from its excited states. The fit employs a data-covariant matrix to take into account the correlation among the time slices in the 50 gauge configurations and is fitted over different ranges of t_f to find the one with the minimum χ^2, much in the same way the hadron masses are fitted. The χ^2 per degree of freedom is small in each of the 3 cases considered here. They are given in Fig. 5. The resultant fits covering the ranges of t_f with the minimum χ^2 are plotted in Fig. 5. Finally, the errors on the fit, also shown in the figure, are obtained by jackknifing the procedure. We see that the slopes are negative in the case of the axial current, in marked contrast to the scalar current in Fig. 4.

In order to compare our results with experiments, we perform the extrapolation to the chiral limit. Plotted in Fig. 6 are the results of $g^1_{A,dis}$ for a single flavor with the same sea-quark mass (denoted as κ_1) as those of the valence- (and cloud-) quarks in the nucleon (κ_2). These results include the one-loop renormalization constant Z_A as in the CI. The DI has a two-loop log divergence in the continuum from the triangle diagram insertion on a quark line [5]. We computed the finite lattice renormalization associated with this 2-loop contribution and found it to be much smaller than the one-loop result. Hence, we have neglected it here. The extrapolation is done with the covariant matrix to consider the correlation among the 3 $\kappa' s$. The error on the chiral limit result is again obtained by jackknifing the procedure of the extrapolation. To calculate Δs (the strangeness contribution to $g^1_{A,dis}$, we fix κ_1 (sea-quark mass) at 0.154 and extrapolate κ_2 (valence-quark mass) to the chiral limit. These results are plotted in Fig. 7.

From Fig. 6 and Fig. 7, we find that $\Delta u_{dis} = \Delta d_{dis} = -0.12 \pm 0.01$ and $\Delta_s = -0.12 \pm 0.01$. Together, we obtain $g^1_{A,dis} = -0.36 \pm 0.03$. Combined with $g^1_{A,con}$, we finally obtain $g^1_A = 0.25 \pm 0.12$ which is in good agreement with experiments [1, 2]. We tabulate these and other results in Table 1 and compare with experiments. We find that they all are in good agreement with experiments. We should mention that our calculation on g^1_A is in agreement with a recent similar calculation with the volume source [20] which predicts $g^1_A = 0.18(10)$. However, their g^3_A, g^8_A, F_A, and D_A are smaller than ours and the experiments by $\sim 20\%$. This presumably is attributable to the fact that their lattice spacing at $\beta = 5.7$ is about 45% larger than ours at $\beta = 6.0$. We would like to point out an interesting observation. Comparing Fig. 6 ($\kappa_1 = \kappa_2$) and Fig. 7 (κ_1 fixed at 0.154, the strange quark mass), we notice that although the sea-quark mass (related to κ_1) changes by a factor of 3 in Fig. 6, the results still coincide with those in Fig. 7 for each of the valence-quark case. It shows that the DI depends sensitively on the valence quark mass but is independent of the sea-quark mass in the loop within errors. This is reminiscent of the finding that, after the finite ma correction for the Wilson action, the coupling between would-be U(1) Goldstone bosons is independent of the mass in the two γ_5 loops [14] for light quarks. The two currents are related to each other via the anomalous Ward identity and, in this context, the mass independence is consistent with a DI of γ_5 current being

dominated by the zero modes. It would certainly be interesting to try to verify this with an explicit calculation of the zero modes.

Table 1: Axial coupling constants and quark spin contents of proton in comparison with experiments

	This Work	Experiments	
$g_A^1 = \Delta u + \Delta d + \Delta s$	0.25(12)	0.22(10) [1]	0.27(10)[2]
$g_A^3 = \Delta u - \Delta d$	1.20(10) [11]	1.2573(28)	
$g_A^8 = \Delta u + \Delta d - 2\Delta s$	0.61(13)	0.579(25) [15]	
Δu	0.79(11)	0.80(6)[1]	0.82(6)[2]
Δd	- 0.42(11)	- 0.46(6)[1]	- 0.44(6) [2]
Δs	- 0.12(1)	- 0.12(4)[1]	- 0.10(4) [2]
$F_A = (\Delta u - \Delta s)/2$	0.45(6)	0.459(8) [15]	
$D_A = (\Delta u - 2\Delta d + \Delta s)/2$	0.75(11)	0.798(8) [15]	
F_A/D_A	0.60(2)	0.575(16) [15]	

In summary, we have computed both the connected and disconnected insertions of the axial current in the proton in a quenched lattice calculation. Albeit they all agree with experiments, the systematic errors due to finite volume, discretization, renormalization, and quenched approximation (which could be as large as 7% – 20%[12]) will have to be addressed in the future. Nevertheless, the physical picture of g_A^1 is getting clearer. The smallness of the quark spin content compared to the non-relativistic value of unity is, first of all, due to the fact that the combined relativistic effect and polarization of the cloud-quarks reduces the CI to 0.62 ± 0.09, a value very close to g_A^8, i.e. $g_{A,con}^1 \simeq g_A^8$. This is because the DI is almost independent of the flavors u, d, and s. Furthermore, the sea-quark polarization is large and in the opposite direction of the proton spin. It is the sum of all these effects that produces a small g_A^1. We should stress that our calculation is gauge-invariant in that no gauge fixing is applied. Since there is no gauge-invariant dimension-three axial operator for the non-abelian gauge field [21, 17], our result is not mixed with the gluon spin. Only the quark spin content contributes. In this paper, we have not attempted to determine the complete composition of the proton spin. That would entail calculations of the orbital angular momentum and the gluon spin, which we leave for a future investigation.

This work is partially supported by DOE Grant DE-FG05-84ER40154. The authors wish to thank T. Draper, C. McNeile, A. Shapere, and C. Thron for helpful comments.

References

[1] D. Adams et al. (SMC), Phys. Lett. **B329**, 399 (1994).

[2] K. Abe et al. (E143), Phys. Rev. Lett. **74**, 346 (1995).

[3] J. Ashman et al. (EMC), Phys. Lett. **B206**, 364 (1988).

[4] S.J. Brodsky, J. Ellis, and M. Karliner, Phys. Lett. **B206**, 309 (1988).

[5] J. Kodaira, Nucl. Phys. **B165**, 129 (1980).

[6] For reviews, see for example S.D. Bass and A.W. Thomas, J. Phys. **G19**, 925 (1993); J. Ellis and M. Karliner, Talk at PANIC '93, hep-ph/9310272; T.P. Cheng and L.F. Li, DPF Conf. '90, 569 (1990).

[7] K.F. Liu, Phys. Lett. **B281**, 141 (1992).

[8] R. Gupta and J.E. Mandula, Phys. Rev. **D50**, 6931 (1994).

[9] R. Altmeyer, M. Göckler, R. Horsley, E. Laermann, and G. Schierholz, Phys. Rev. **D49**, R3087 (1994).

[10] T. Draper, R.M. Woloshyn and K.F. Liu, Phys. Lett. **234B**, 121 (1990); W. Wilcox, T. Draper, and K.F. Liu, Phys. Rev. **D 46**, 1109 (1992).

[11] K.F. Liu, S.J. Dong, T. Draper, J.M. Wu, and W. Wilcox, Phys. Rev. **D 49**, 4755 (1994).

[12] K.F. Liu, S.J. Dong, T. Draper, and W. Wilcox, Phys. Rev. Lett. (to appear); UK/94-01, hep-lat/9406007.

[13] G.P. Lepage and P.B. Mackenzie, Phys. Rev. **D48**, 2250 (1993).

[14] J.F. Lagaë and K.F. Liu, UK/94-04, hep-lat/9501007.

[15] F.E. Close and R.G. Roberts, Phys. Lett. **B316**, 165 (1993).

[16] K.F. Liu and S.J. Dong, Phys. Rev. Lett. **72**, 1790 (1994).

[17] R.L. Jaffe and A. Manohar, Nucl. Phys. **B337**, 509 (1990).

[18] L. Maiani et al., Nucl. Phys. **B293**, 420 (1987).

[19] S.J. Dong and K.F. Liu, Phys. Lett. **B328**, 130 (1994).

[20] M. Fukugita, Y. Kuramashi, M. Okawa, and A. Ukawa, KEK preprint 94-173, hep-lat/9501010.

[21] C. Cronström and J. Michelsson, J. Math. Phys. **24**, 2528 (1983).

Figure Captions

Fig. 1 (a) The connected insertion. (b) The disconnected insertion.

Fig. 2 The lattice $g_{A,con}^{1L}$ for the connected insertion as a function of the quark mass ma. The chiral limit result is indicated by $\bullet$.

Fig. 3 The ratio $R_A = g_A^1/g_A^3$ for the CI is plotted as a function of ma. The results of the valence approximation are shown as $\bullet$.

Fig. 4 The ratios in eq.(5) are plotted for the vector, pseudoscalar, and scalar currents with quark masses $\kappa = 0.148$ and 0.154. ME gives the fitted slope.

Fig. 5 The ratios of eq.(5) for the axial current are plotted for the 3 κ cases. ME is the fitted slope.

Fig. 6 The DI of the axial current as a function of ma. The quark masses in the valence and the sea are kept the same. The chiral limit result is indicated by $\bullet$.

Fig. 7 The same as in Fig. 6 except the sea quark mass (κ_1) is fixed at 0.154.

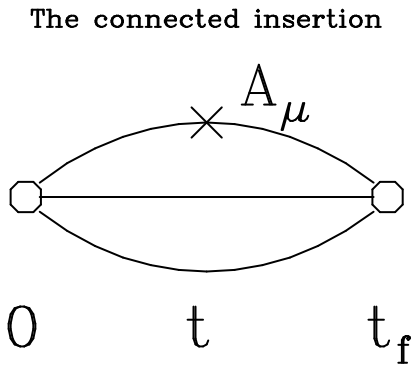

Fig.1a

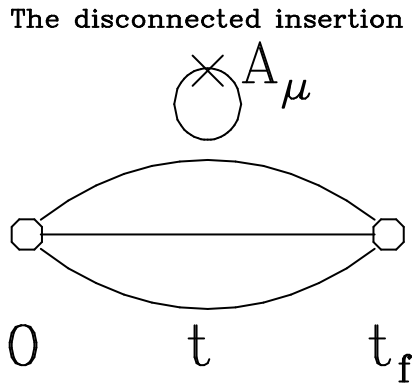

Fig.1b

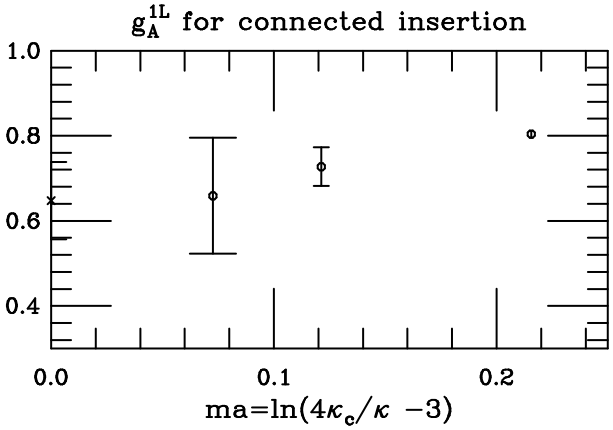

Fig.2

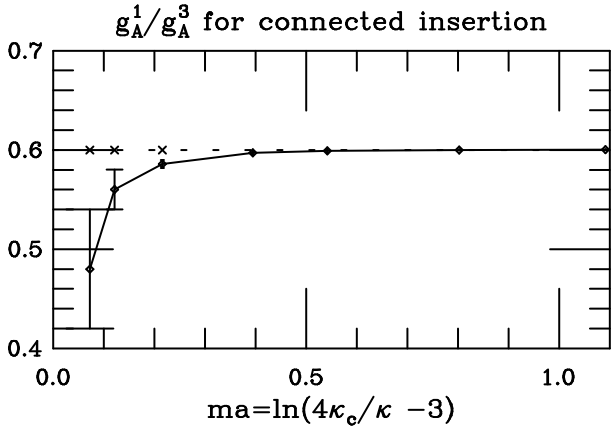

Fig.3

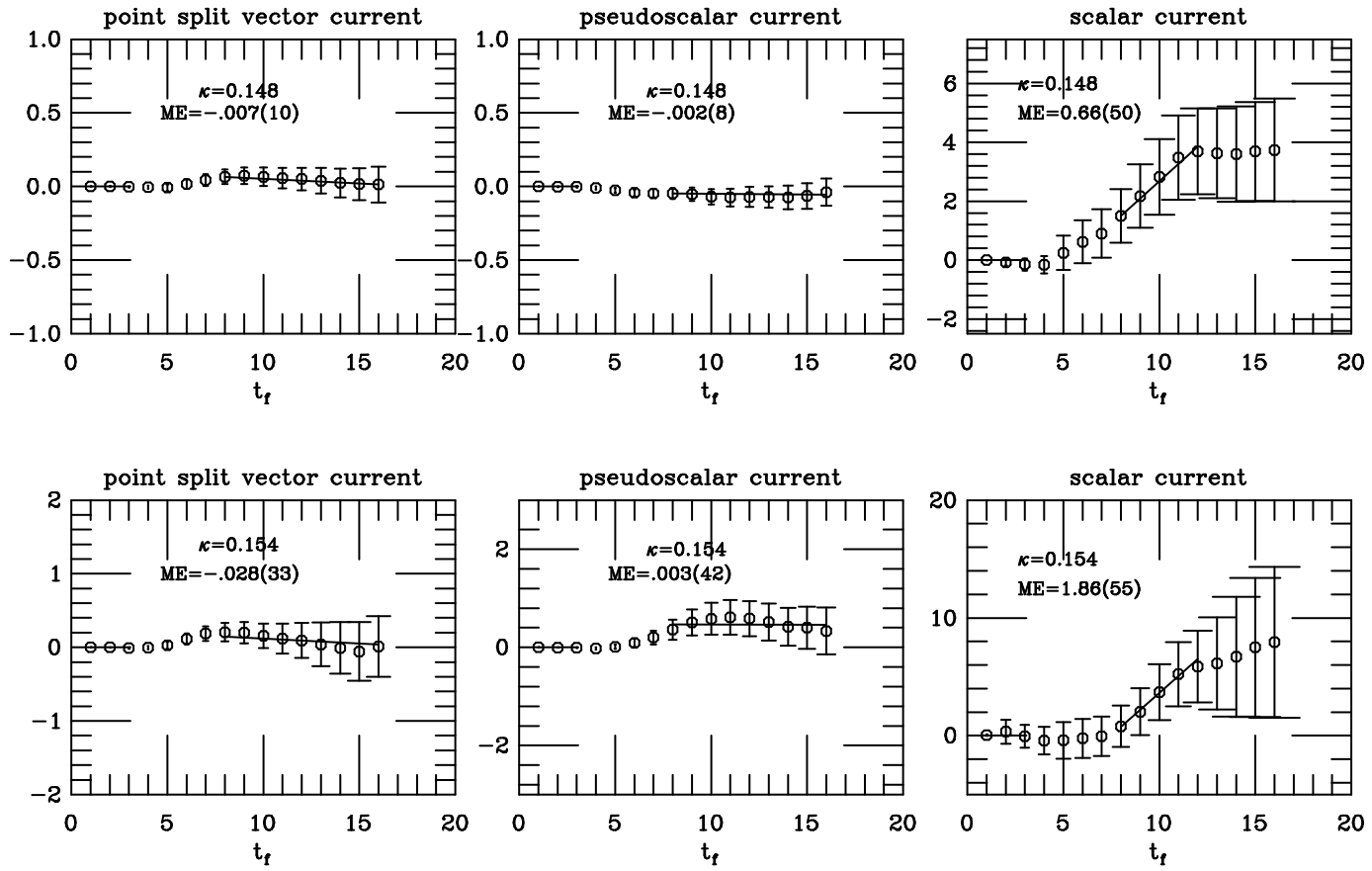

Fig.4

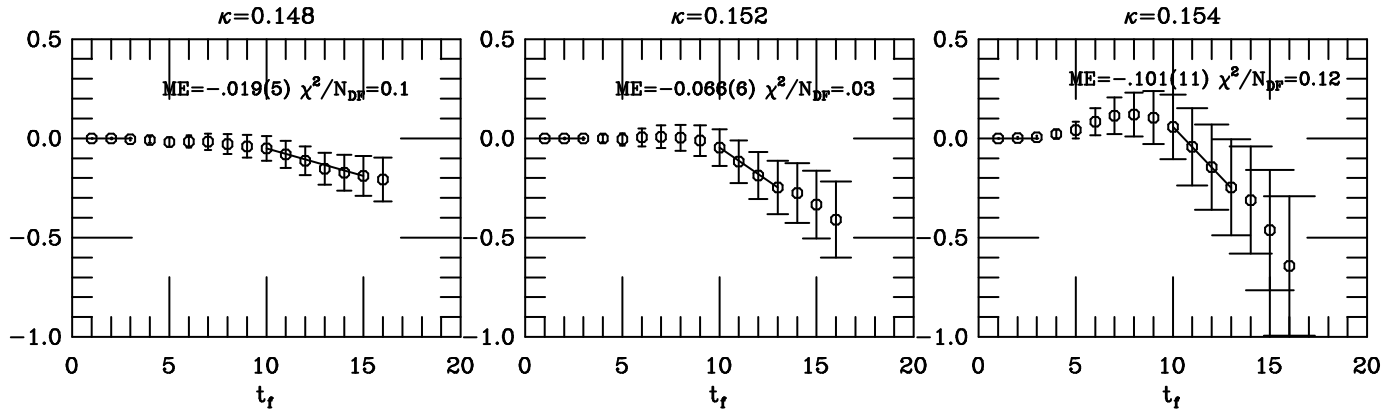

Fig.5

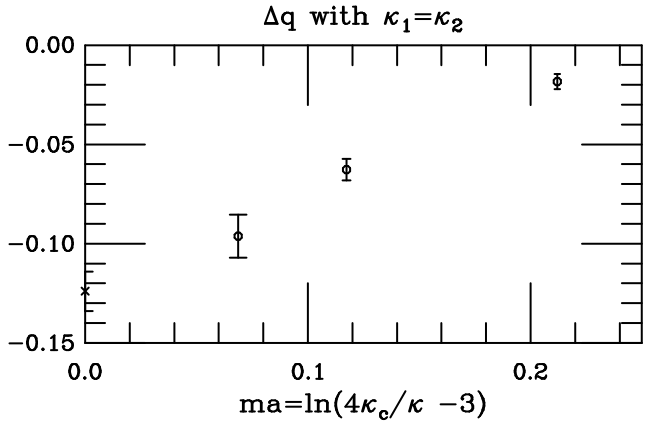

Fig.6

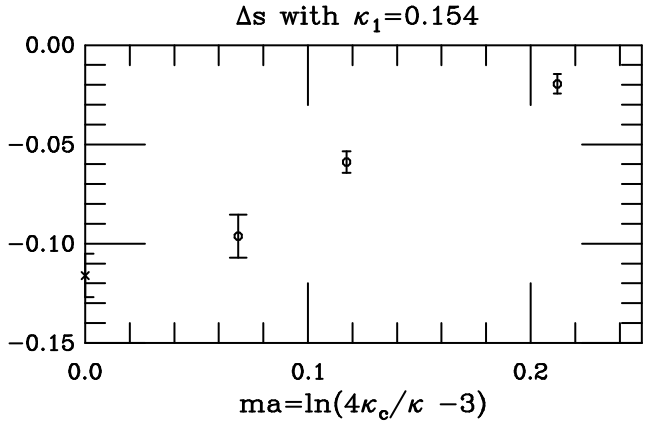

Fig.7